ACS APPLIED MATERIALS & INTERFACES

Research Article

Cite This: ACS Appl. Mater. Interfaces 2018, 10, 17107−17116

www.acsami.org

Clickable-Zwitterionic Copolymer Capped-Quantum Dots for in Vivo Fluorescence Tumor Imaging

Laura Trapiella-Alfonso,[†,‡,§,∥,⊥,¶] Thomas Pons,[⊥] Nicolas Lequeux,[⊥] Ludovic Leleu,[†,‡,§,∥] Juliette Grimaldi,[†,‡,§,∥,⊥] Mariana Tasso,[⊥,#] Edward Oujagir,[‡,§,∥] Johanne Seguin,[‡,§,∥] Fanny d'Orlyé,[†,‡,§,∥] Christian Girard,[†,‡,§,∥] Bich-Thuy Doan,[†,‡,§,∥] and Anne Varenne*[,†,‡,§,∥]

[†]PSL Research University, Chimie ParisTech, Unité de Technologies Chimiques et Biologiques pour la Santé, 75005 Paris, France

[‡]INSERM, Unité de Technologies Chimiques et Biologiques pour la Santé (U 1022), 75006 Paris, France

[§]CNRS, Unité de Technologies Chimiques et Biologiques pour la santé UMR 8258, 75006 Paris, France

[∥]Université Paris Descartes, Sorbonne Paris Cité, Unité de Technologies Chimiques et Biologiques pour la Santé, 75006 Paris, France

[⊥]Laboratoire de Physique et d'Étude des Matériaux (LPEM), ESPCI Paris, PSL Research University; CNRS; Sorbonne Universités, UPMC Univ. Paris 6, 10 rue Vauquelin, F-75231 Paris Cedex 5, France

Supporting Information

ABSTRACT: In the last decades, fluorescent quantum dots (QDs) have appeared as high-performance biological fluorescent nanoprobes and have been explored for a variety of biomedical optical imaging applications. However, many central challenges still exist concerning the control of the surface chemistry to ensure high biocompatibility, low toxicity, antifouling, and specific active targeting properties. Regarding in vivo applications, circulation time and clearance of the nanoprobe are also key parameters to control the design and characterization of new optical imaging agents. Herein, the complete design and characterization of a peptide-near-infrared-QD-based nanoprobe for biomedical optical imaging is presented from the synthesis of the QDs and the zwitterionic-azide copolymer ligand, enabling a bio-orthogonal coupling, till the final in vivo test through all the characterization steps. The developed nanoprobes show high fluorescence emission, controlled grafting rate, low toxicity, in vitro active specific targeting, and in vivo long circulating blood time. This is, to our knowledge, the first report characterizing the in vivo circulation kinetics and tumor accumulation of targeted zwitterionic QDs.

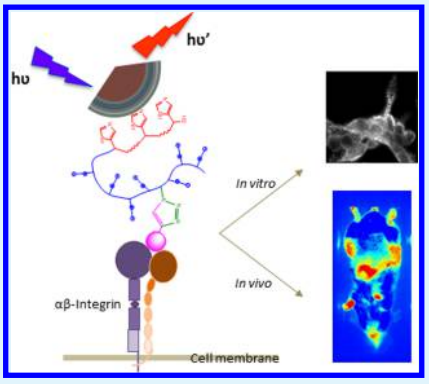

KEYWORDS: *zwitterionic copolymers, near-infrared quantum dots, click chemistry, RGD peptide, capillary electrophoresis, optical imaging, cancer diagnosis*

1. INTRODUCTION

Semiconductor quantum dots (QDs) represent an interesting class of fluorescent nanoparticles with exciting optical features such as their narrow tunable emission spectra, high brightness, and photostability.[1] Since their first application in fluorescence microscopy, they have been used for many applications such as tracking of single molecule in living cells[2,3] or performing multiplexed fluorescent immunostaining.[4] Near infrared (NIR) emitting QDs have also been used for in vivo imaging, taking advantage of the lower absorption and deeper penetration of NIR light into tissues compared to visible light.[5,6] In particular, $CuInS_2$- and $CuInSe_2$-based QDs have recently emerged as a bright, less-toxic alternative to the first generation of NIR QDs based on cadmium, lead, or mercury chalcogenides.[7−9] The emission of these nanoprobes can be tuned throughout the NIR range (700−1000 nm) and display good fluorescence quantum yield, up to 30−40%. In addition, they possess special optical properties such as long fluorescence lifetimes, enabling the use of time-gated detection to reduce the autofluorescence background and increase imaging sensitivity.[10]

While the optical properties of these QDs have been optimized over the years to yield stable and bright probes, their in vivo fate is mostly governed by their surface chemistry and their interactions with biological molecules or membranes. Early generations of QDs were stabilized by amphiphilic molecular surfactants or copolymers; however, these surface chemistries lacked stability and were prone to nonspecific interactions.[11] This led to fast elimination from the blood stream because of opsonization and capture by macrophages of the reticuloendothelial system, thereby limiting their in vivo imaging capacity.[12−14] Another alternative consisted in exchanging the initial hydrophobic surface ligands by new hydrophilic ligands, but small monodentate ligands were also

Received: March 23, 2018
Accepted: April 27, 2018
Published: April 27, 2018

DOI: 10.1021/acsami.8b04708
ACS Appl. Mater. Interfaces 2018, 10, 17107−17116

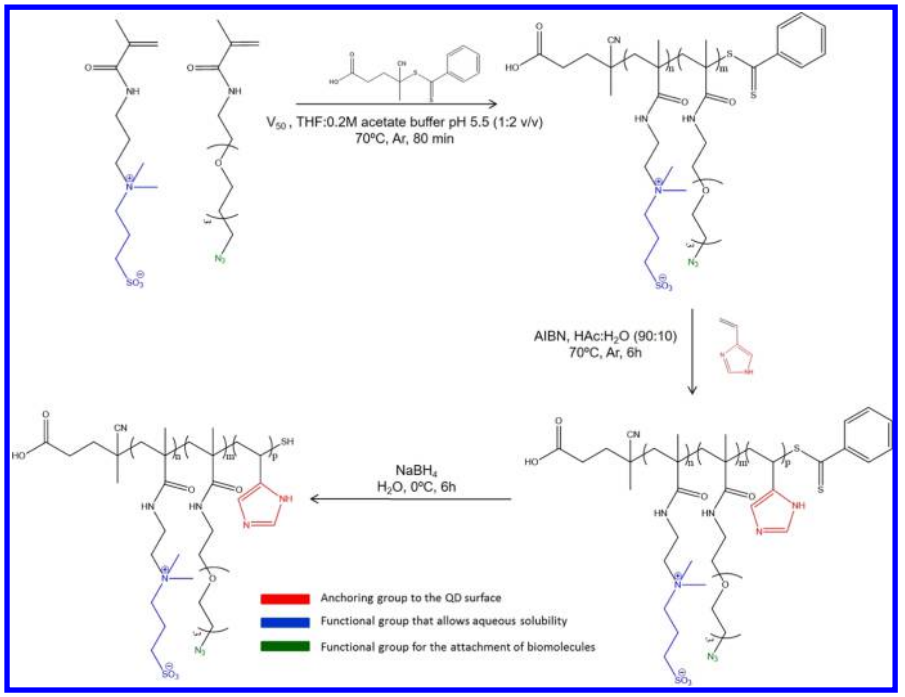

Figure 1. Synthesis of the zwitterionic block copolymer azido-sulfobetaine-4-vinylimidazole in three steps: first, a RAFT polymerization of the monomers *N*-(11-azido-3,6,9-trioxaundecan)metacrylamide and methacrylamidosulfobetaine; a second step of block polymerization with 4-vinylimidazole; followed by the final reduction step to liberate the RAFT moiety. In red is represented the functional group to anchor to the QD surface, in blue the zwitterion that provides the aqueous solubility and antifouling properties, and in green the azide function to enable further biofunctionalization.

prone to fast desorption. Recently, more robust surface chemistries have been developed, which incorporate several anchoring groups within a polymeric ligand to enhance the affinity of the ligands for the QD surface.[15−18] This increased affinity strongly reduces ligand desorption and yields QDs that are stable for long periods of time in dilute conditions and in complex environments, such as the intracellular medium. In particular, zwitterionic polymers are attracting increasing interest, thanks to their demonstrated antifouling properties, leading to a better nanoprobe performance in bioapplications.[19−23] However, up to now, the studies carried out have been restricted to in vitro assays and cellular imaging.[24,25] While polyethylene glycol-coated nanoparticles have been extensively studied for in vivo applications, there is only limited insight on the in vivo behavior of zwitterion-coated inorganic nanoprobes.[26,27]

Another important parameter is the ability to conjugate targeting agents to the surface of the QDs with a good control over their orientation to maintain their structural integrity and functionality. This can be achieved through the use of bio-orthogonal coupling strategies such as the azide−alkyne click chemistry.[28]

In this study, we report the synthesis and characterization of a novel block copolymer composed of a first block of vinylimidazole for strong anchoring to the QD surface and a second block of sulfobetaine- and azido-monomers to ensure solubility and antifouling and to enable further bio-orthogonal click chemistry. This clickable zwitterionic polymer is obtained by controlled radical polymerization that yields monodisperse polymeric ligands. We first characterized the physicochemical properties of QDs capped with this new copolymeric ligand. We then demonstrated the efficient azide−alkyne conjugation on these QDs. We applied this conjugation scheme to couple arginylglycylaspartic acid (RGD) peptides at the surface of the QDs. This peptide motif is able to recognize $\alpha_v\beta_3$ integrin, an important adhesion transmembrane protein, that is overexpressed in several cancers and plays an important role in angiogenesis. We demonstrated that the obtained RGD-QDs are able to specifically label $\alpha_v\beta_3$ integrin-expressing cell lines in vitro, and we tested the in vivo imaging capacity of these novel nanoprobes in a CT26 tumor mouse model, characterizing for the first time the in vivo circulation kinetics and tumor accumulation of zwitterionic NIR-QDs.

2. MATERIALS AND METHODS

Unless otherwise specified, all reagents were used as received. Deionized ultrapure water (resistivity 18.2 MΩ·cm) was used throughout the work.

2.1. Synthesis of QD Nanoparticles. Two kinds of QDs were used in this work: (1) CdSe/CdS/ZnS core/multishell QDs emitting at 620 nm (vis-QDs, for optimizations and in vitro assays) and (2) ZnCuInSe/ZnS core/shell QDs emitting at 800 nm (NIR-QDs, for in vivo experiments). Both types of QDs share the same outer ZnS shell, which enables using the same surface chemistry and functionalization schemes. The syntheses of both kinds of QDs following methodologies already reported[10,29,30] are described in the Supporting Information, and their optical properties (excitation/emission spectra, lifetimes, and colloidal stability) are collected in Figure S1.

2.2. Synthesis of Zwitterionic Block Copolymer. Two zwitterionic block polymers [a homopolymer poly(methacrylamidosulfobetaine-*block*-4-vinylimidazole) named P(SPP-4VIM); a copolymer introducing a monomer with the azido clickable function, named throughout the work P(SPP-N_3-4VIM)] were synthesized following the reversible addition−fragmentation chain transfer (RAFT) polymerization approach (see the synthesis route in Figure 1). The procedure carried out to prepare these polymers is detailed in Tasso et al.[25] In the case of the block copolymer synthesis, the monomers (azido function/SPP) molar ratio was fixed at 1/7 (see the Supporting Information for the synthesis and characterization of

DOI: 10.1021/acsami.8b04708
ACS Appl. Mater. Interfaces 2018, 10, 17107−17116

the azido-monomer). Because of the poor solubility of the N_3-monomer in aqueous buffer, it was first solubilized in a minimum volume of an organic solvent [tetrahydrofuran (THF)]. THF was already proved to be compatible with the synthesis of this kind of zwitterion polymers.[20] After the polymerization to recover the polymers, several precipitation purification steps were performed. The polymer was precipitated in cold acetone, redispersed in water, and precipitated in EtOH three times. Finally, the solid was dried under vacuum overnight. This first polymer block was characterized by gel permeation chromatography in water (Viscotek GPCmax, triple detection). The presence of the azido function in the clickable zwitterionic block copolymer was confirmed by Fourier transform infrared spectroscopy (FT-IR), identifying the corresponding characteristic peak at 2100 cm^{-1} (see Figure S2). Finally, capillary electrophoresis was used to follow the whole process of synthesis to provide the global surface charge density and the size homogeneity of the final polymer.

2.3. Peptide Derivatization. c-(RGDfK) active peptide for $\alpha_v\beta_3$ integrin targeting and c-(RADfK) selected as the control peptide were purchased from Eurogentec (Angers, France), and their structures are displayed in Figure S3A [note that they only differ in a methyl group (signaled in orange in the chemical structure) because of the exchange of the G amino acid by A amino acid]. As it can be seen, to be able to click these peptides to QDs a preliminary derivatization step is required to introduce an alkyne function in their structures. For such purpose and considering the special conditions (water medium and free of Cu) where the further QDs click coupling will be performed, the dibenzocyclooctyne-*N*-hydroxysuccinimidyl ester (DBCO-NHS) molecule was selected for peptide derivatization (see its structure in Figure S3B). The peptide derivatization takes place between the primary amine of the lysine amino acids (in blue) from the peptide and the carboxylic ester group (in red) of the DBCO-NHS. c-(RGDfK) and c-(RADfK) peptides were reacted with a DBCO-NHS linker in a peptide−DBCO-NHS molar ratio of 1:1, in a 0.1 M Na_2HCO_3/NaH_2CO_3 buffer at pH 8.3, during 2 h at room temperature under vertical/horizontal mechanical rotation. The product was precipitated in acetone and dried under vacuum. The peptide was then dispersed in dimethyl sulfoxide (10 mg mL^{-1} stock solution) aliquoted and stored in the freezer (−20 °C). The DBCO−peptide structure is presented in Figure S3C. It was further characterized by MS and NMR.

2.4. Click Chemistry Coupling: Peptide/QD Bioconjugates. This bio-orthogonal coupling between the azide functions present at the surface of P(SPP-N_3-4VIM)-coated QDs and the alkyne groups from DBCO−peptides is carried out in a 20 mM NaCl solution, working with a QD/peptide molar ratio of 1:100 and incubating overnight at room temperature with continuous mechanical rotation (a reaction scheme is presented in the Supporting Information, Figure S4). Purification from free unbound peptides is performed by five cycles of ultrafiltration using Vivaspin filters (100 kDa cut-off, 13 000*g*, 8 min). The final peptide-modified QDs were stored in 20 mM NaCl solution in the fridge until use. Control peptide-free QDs were obtained by incubating P(SPP-N_3-4VIM)-coated QDs with DBCO-NHS overnight at a QD/DBCO-NHS in a high excess molar ratio of 1:500 to ensure the complete replace of azido function by carboxylic ones (after hydrolysis of the NHS ester) and then to limit nonspecific interactions due to the $-N_3$ moieties. Control QDs were purified using the same procedure as RGD- and RAD-QDs.

2.5. Characterization by Capillary Electrophoresis. Electrophoretic measurements were performed with a 7100 capillary electrophoresis system equipped with a diode-array and Zetalif fluorescent detectors (Agilent Technologies, Waldbronn, Germany). Data were handled with ChemStation. Bare fused-silica capillaries of 50 μm inner diameter (Polymicro Technologies, Phoenix, AZ, USA) with an effective length of 8.5 and 21.0 cm for UV and fluorescent detection, respectively, and a total length of 35.0 cm were used. Two different methodologies were employed during this work: (1) capillary zone electrophoresis (CZE) for the physicochemical characterization of both polymers and QDs and (2) affinity capillary electrophoresis (ACE) for the evaluation of possible interactions of QDs with proteins [using bovine serum albumin (BSA) as a model to check the nonspecific interactions or the antifouling properties of the QD's surface chemistry]. Two background electrolytes (BGEs) were used along the work: carbonate buffer $NaHCO_3/Na_2HCO_3$ pH 9.5, a good solvent for sulfobetaine-vinylimidazole grafted-QDs, and 40 mM (3-(*N*-morpholino)propanesulfonic acid) (MOPS) buffer pH 7.4 to mimic the physiological environment. A study of the effect of ionic strength of the media (10−100 mM) was performed with the carbonate buffer. Note that 20 mM NaCl solution was systematically added to BGE to ensure the stability of the samples.

A solution of 1‰ of *N*,*N*-dimethylformamide was used as a neutral marker (NM) through the work. A first dilution to 1% (vol %) was prepared in ultrapure water, and then, the final dilution was made with the corresponding BGE. The NM solution was renewed every day. For CZE experiments, successive hydrodynamic injections were performed in the following order: NM (30 mbar, 3 s), BGE (30 mbar, 3 s), sample (30−50 mbar, 3−5 s, according to cases), BGE (30 mbar, 3 s). In the case of ACE analysis, the BGE was enriched with BSA in the 0−20 μM concentration range. Separations were performed under +10 kV and the temperature of the capillary cartridge was set at 25 °C. The detection wavelengths were 200, 214, 254, and 280 nm for UV−vis detection and 480 nm as the excitation wavelength with a band-pass filter for emission centered at 500 nm for fluorescence detection. Injections were repeated at least three times to evaluate data reproducibility. Prior to first use, bare fused-silica capillaries were activated by successive rinsing with 1 M NaOH solution for 15 min, followed by 0.1 M NaOH solution, 0.01M NaOH solution, and ultrapure water for 10 min each under 925 mbar. Between each run, the capillary was rinsed with BGE for 3 min under the aforementioned pressure. When not in use, the capillaries were rinsed with ultrapure water for 10 min and dried with air for 5 min.

2.6. Cellular Viability Test (MTT). The effect of both kinds of synthesized QD surface-functionalized with the two types of zwitterion block co-polymers over the metabolism of HeLa cells in culture was evaluated in parallel. In a typical test, HeLa cells were seeded into 96-well plates at 25 000 cells mL^{-1} (100 μL/well) to reach a 70% cell confluence level by the end of the incubation period (24 h). Twenty-four hours after seeding, the cells were washed once with Dulbecco's phosphate-buffered saline and exposed to 100 μL of QDs dispersed in the culture medium at different concentrations (0.03−5 μM). Two different QD conditions were considered in triplicate: (i) P(SPP-N_3-4VIM) block copolymer vis-QDs; (ii) P(SPP-N_3-4VIM) block copolymer NIR-QDs. Control wells with only cells (blank) were also included. Additional controls without cells were: (i) a blank well with only cell medium and (ii) a control with the highest evaluated nanoparticle concentration in cell medium. This latter control intended to assess eventual (and parasitic) MTT false readings induced by unwashed, unspecifically adsorbed QD nanoparticles.[31] In our assays, such an effect was not observed: after the MTT reaction, the absorbance of the only-QDs control was similar to the one of the blank with only medium. At the end of the incubation period (24 h), QD suspensions were removed and the cells rinsed once with cell medium. The cells were further incubated for 2 h with 5 μL of MTT solution (5 mg mL^{-1} in water) in 100 μL cell medium to enable the enzymatic conversion of the MTT reagent into water-insoluble, cell-confined blue formazan crystals. Thereafter, the MTT solution was aspirated and the wells were let to dry briefly. To resuspend the formazan crystals, the cells were lysed by exposure to 100 μL of a 9:1 isopropanol/Triton X-100 and 0.1% HCl solution for 15 min. Formazan concentration was determined via absorbance measurement at 550 nm in a standard plate reader.

2.7. In Vitro Study of the Nanoprobe: Cellular Binding Tests. These experiments were carried out into a 4-chamber Lab-Tek II #1.5 cover glass system as support. Two cell lines were tested CT26 mouse carcinoma fibroblast cell line (overexpressing the integrin) and NIH3T3 mouse fibroblast cell line as a control. Four different modified-QDs were tested to demonstrate the specific targeting: (i) P(SPP-4VIM) QDs; (ii) P(SPP-N_3-4VIM) QDs; (iii) RGD-QDs; and (iv) RAD-QDs; where (i) and (ii) are the QD surface chemistry controls, (iii) is the specific positive peptide, and (iv) is the control/

DOI: 10.1021/acsami.8b04708
ACS Appl. Mater. Interfaces 2018, 10, 17107−17116

negative peptide. The working solutions of these QDs were prepared in the cell culture medium (Dulbecco's modified Eagle's medium supplemented with 10 vol % fetal bovine serum and 1 vol % of 10 000 U mL^{-1} penicillin−streptomycin). Several optimizations of the test were made to ensure the best conditions for the specific integrin (tumor) targeting including concentration of the nanoprobe, saturation step, incubation temperature and time, washing solution, among others. The fluorescent images were taken in an Olympus IX71 wide-field epifluorescence microscope with a Cascade II 512 EMCCD camera in the following configuration: 60× objective, 425/60 nm excitation and 625/40 nm emission band-pass filters, 500 ms exposition time, gain 3, intensifier 1. Finally, the images were analyzed with ImageJ software.

The finally selected protocol is described below. The CT26 and NIH3T3 cells were seeded (500 μL/well at 200 000 cells mL^{-1}) in the 4-chamber Lab-Tek II support and incubated 24 h at 37 °C, 5% CO_2, for their proliferation until confluence (70%). The media was sucked up and 500 μL/well of the corresponding working solution were added and incubated 1 h at 4 °C. After that, the solutions were removed and the support was washed twice with the washing solution (0.9% NaCl/1 mM $CaCl_2$/0.05% Tween 20; 800 μL/well) and once with washing solution free of Tween 20. Then, 500 μL/well of 4 vol % paraformaldehyde in NaCl solution were added to fix the cells and the support was incubated 10 min at 4 °C protected from the light. The plate was washed twice with the washing solution free of Tween 20. Finally, 500 μL/well of 0.9% NaCl solution was introduced, and imaging was performed using the fluorescence microscope.

2.8. In Vivo Study of Peptide-Modified NIR-QDs. These experiments deal with the assessment of in vivo biodistribution, specific targeting, uptake, kinetics, and clearance of the newly developed optical imaging agents. The experiments were carried out in two sets: (i) control no-peptide-NIR-QDs (passive targeting) and (ii) peptide-modified NIR-QDs (active/negative targeting). This work has been submitted for ethical evaluation to the Paris-Descartes Ethics Committee for Animal Research. It was approved by the Committee, and its registered number is CEEA34.JS.142.12. To perform these studies, healthy and tumor-induced BALBc/JRJ 6 week female mice were used. To induce the CT26 tumor in the mice, two bilateral subcutaneous implantations of a fragment of CT26 tumor were performed in the flank.[32] Imaging experiments were performed after 14 days of tumor growth using the photonIMAGER Optima instrument and PhotoAcquisition software, both from Biospace Lab. After the optimization for the collection of the fluorescent images, the acquisitions were carried out in the following configuration: excitation filter at 637 nm (bandpass filter), background filter at 487 nm (bandpass filter), and emission filter at 800 nm (high-pass filter), with a whole duration of 5 s. Before each experiment, the fluorescence emission of the nanoprobe solution and an image of the mice before injection were acquired (see the Supporting Information, Figure S5). All the dilutions of the nanoprobe solution were made with physiological serum. After the intravenous injection of the nanoprobe via the tail vein (100 μL, 7 μM), the images were collected at the following time intervals: 1, 5, 15, 30 min, 1, 2, 3, 4, 5, 6, and 24 h. Images were postprocessed using M3 Vision Biospace software.

3. RESULTS AND DISCUSSION

3.1. Synthesis and Characterization of Zwitterionic Block Co-Polymer P(SPP-N_3-4VIM). A methacrylamide monomer was prepared with a terminal azide function and a three-ethylene glycol linker by the reaction of 11-azido-3,6,9-trioxaundecan-1-amine with methacryolyl chloride (see the Supporting Information). Then, this azide-terminated monomer was used to prepare a P(SPP-N_3-4VIM) block copolymer by RAFT polymerization as shown in Figure 1. The first block of this polymer is composed of a statistical copolymer of sulfobetaine monomers (for solubilization and antifouling) and azide monomers (for further click chemistry bioconjugation). The second block is composed of imidazole monomers to provide strong multidentate anchoring to the QD surface.[25] GPC analysis yielded a number-average molar mass (M_n) of 14 kDa with a polydispersity index (PDI) of 1.1 for the first block of the polymer P(SPP-N_3). Considering the initial ratio between both monomers for the polymerization and their respective molecular weights, this result suggests that an average of 39 monomers of SPP and 6 monomers of N_3 are present in the final polymer chain (see calculations in the Supporting Information). The analysis of the final polymer by GPC is not possible because of interactions between the imidazole block and the available stationary phase. All the steps of the polymer synthesis as well as the final product were analyzed by CZE to characterize the global charge density and size homogeneity of the final polymer (results are collected in the Supporting Information, Table S1). As the characterization was performed in aqueous media at 25 °C, the equation of Helmholtz−Smoluchowski (a modification of Henri's equation) was used to calculate the ζ-potential using the mobility values. The values of PDI were obtained by the increment of mobility ($\Delta\mu$) measured at 10% of signal intensity from the background divided by the electrophoretic mobility measured at the peak center. We note that P(SPP-4VIM) and P(SPP-N_3-4VIM) are comparable in size and that both have a slight global negative charge under these experimental conditions given by similar electrophoretic mobilities (6.0 ± 0.7 and $6 \pm 1 \times 10^{-5}$ $cm^2\ V^{-1}\ s^{-1}$, respectively). Addition of the azide monomer does not significantly modify the mobility nor the ζ-potential, which is in accordance with its structure. Even the polydispersity of the sample characterized here by the PDI remains stable during the process (going from 1.5 ± 0.5 of the initial sulfobetaine reagent to 2 ± 1 of the final polymer) and being similar to that obtained by GPC.

3.2. Synthesis, Solubilization, and Biofunctionalization of QDs. Two kinds of QDs were used in this work, namely visible-emitting CdSe/CdS/ZnS and NIR-emitting ZnCuInSe/ZnS core/shell QDs. As mentioned above, NIR-QDs were selected for in vivo experiments to overcome the limitations of vis-QDs, such as the poor penetration depth and strong tissue autofluorescence in the visible range.[33] Their syntheses were performed in high boiling point organic solvents. After their purification, they were stored in hexane before being transferred to an aqueous phase via a two-step ligand exchange procedure (see the Supporting Information). Their optical emission properties as well as their size were measured as indicators of the synthesized QD quality (see Figure S1). Fluorescence spectra were centered at 620 nm for vis-QDs and 800 nm for NIR-QDs, with average radius around 7 and 4 nm, respectively, as observed by transmission electron microscopy.

QDs were coated with P(SPP-4VIM) or P(SPP-N_3-4VIM) using a two-step ligand exchange process and purified by ultrafiltration and ultracentrifugation. The hydrodynamic radii were 12 and 9 nm, respectively, for vis-QDs and NIR-QDs, as measured by DLS. These water-soluble QDs have typical fluorescence quantum yields of 40−50% for visible-emitting QDs and 15−25% for NIR-QDs. These QDs show an excellent stability for several months in pH 7 buffer when stored at 4 °C, as well as for 24 h at 37 °C in various biologically relevant saline buffers (pH 6−8) and in culture medium (colloidal stability > 95% and fluorescence stability > 80%, see Figure S1). These QDs show multiexponential fluorescence decay kinetics, with lifetimes of the largest component ca. 20 ns for visible QDs and 260 ns for NIR QDs , as expected for these QD composition

DOI: 10.1021/acsami.8b04708
ACS Appl. Mater. Interfaces 2018, 10, 17107−17116

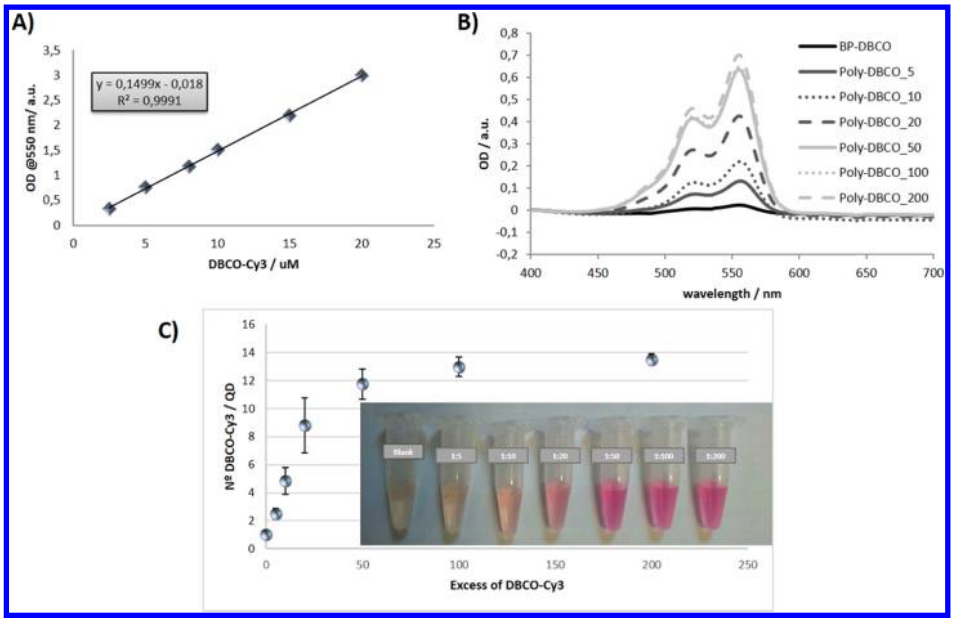

Figure 2. Proof of concept of click chemistry coupling between QDs and DBCO-Cy3. (A) Calibration curve of DBCO-Cy3. (B) Deconvoluted absorption spectra (Cy3 contribution) of different QD/DBCO-Cy3 conjugates. (C) Evolution of the number of Cy3 per QD as a function of the initial DBCO-Cy3/QD molar ratio. Error bars correspond to experimental deviations from three independent replicates. The inset image shows a picture of the solutions corresponding to different DBCO-Cy3/QD molar ratios (from left to right: BP-DBCO; 5, 10, 20, 50, 100, and 200). Note that the BP-DBCO was done with the highest excess of the dye.

and sizes (Figure S1). Finally, further characterization of these QDs and their bioconjugates were carried out by capillary electrophoresis and are discussed below in a special section.

Click chemistry reaction is a Huisgen's [3 + 2] thermal cycloaddition between organic azides and alkynes to create stable covalent bindings by the formation of 1,2,3-triazoles rings.[28] Normally, this reaction is performed using Cu(I) as the catalyst and has already shown its potential for the functionalization of NPs.[34,35] However, Cu(I) efficiently quenches the fluorescence emission of QDs.[36] To avoid the use of Cu(I), cyclooctyne and derivatives have been reported in previous publications as a successful alternative to perform the click chemistry working with QDs.[36−38] Those reported QD conjugates were not used for tumor active targeting or in vivo specific targeting studies; they, however, demonstrated the effectiveness of cyclooctine for bio-orthogonal coupling of biomolecules. Herein, we used dibenzocyclooctyne (DBCO), a stretched activated alkyne which reacts with azide group in copper-free conditions to prepare QD nanoprobes, for specific active tumor targeting in vitro and in vivo (a reaction scheme is presented in Figure S4).

3.2.1. Proof of Concept of the Click Chemistry: Coupling with DBCO-Cy3. The optimization of this specific and selective reaction was first made using the DBCO-Cy3 as the proof of concept. This conjugate was selected because of its similarity in size with our peptide−DBCO (see its structure in Figure S3D) and because it has a distinct absorbance/fluorescence signature from QDs that allows to follow the reaction. Thus, different molar excess of the DBCO-Cy3 (5, 10, 20, 50, 100, and 200) were incubated with P(SPP-N_3-4VIM)-QDs overnight at room temperature to characterize the saturation of the QD surface N_3 sites. A control sample consisting in incubating P(SPP-4VIM)-QDs (azide free) with the highest molar excess of DBCO-Cy3 was also tested. After purification from unbound dyes by ultrafiltration, the absorption spectra of each QD/DBCO-Cy3 conjugate were collected and compared to calibration curves of QD and DBCO-Cy3 alone (Figure 2A). The number of Cy3 per QD was estimated by deconvoluting absorption spectra and measuring the absorbance of the dye contribution (Figure 2B). Saturation is reached for >50 DBCO-Cy3/QD initial molar excess and corresponds to ca. 13 molecules of DBCO-Cy3 conjugated per QD (Figure 2C). Note that in the case of the control QDs without azide functions (black line in Figure 2B) no signal from the DBCO-Cy3 was observed, indicating the absence of nonspecific reaction between P(SPP-4VIM)-QDs and DBCO-Cy3 at the highest concentration tested. This is corroborated by visual inspection of the purified QD solutions after the reaction (Figure 2C, inset).

3.2.2. Peptide Derivatization with DBCO. The selected target peptides c-(RGDfK) and c-(RADfK) were functionalized with DBCO to enable coupling to azide-QDs. To this end, coupling with DBCO-NHS ester was selected because of the easy and effective coupling reaction with the primary amine present in the lysine residue (K) of the peptides, following the protocol described in the Materials and Methods section. The effectiveness of the coupling was confirmed by the ESI−MS analysis of the DBCO-RAD-modified peptide with a m/z of the molecular ion $[M + H]^+$ of 905.6 Da and for the ion $[M + Na]^+$ of 927.9 Da, both in agreement with the expected theoretical molecular weight 904.4 Da. ^{1}H NMR spectra also show peaks coming from both molecules in the final conjugate (see Figure S6), supporting the effective formation of the DBCO−peptide product.

3.2.3. Biofunctionalization of QDs and Characterization by CE. Copper-free click chemistry was then used for the biofunctionalization of P(SPP-N_3-4VIM)-QDs with the two DBCO−peptides, following the protocol described in the Materials and Methods section, leading to RAD-QDs and RGD-QDs. Before biological applications, the four types of nanoprobes [P(SPP-4VIM)-QDs, P(SPP-N_3-4VIM)-QDs, RAD-QDs, and RGD-QDs] were characterized by CZE to better understand their behavior under physiological conditions

DOI: 10.1021/acsami.8b04708
ACS Appl. Mater. Interfaces 2018, 10, 17107−17116

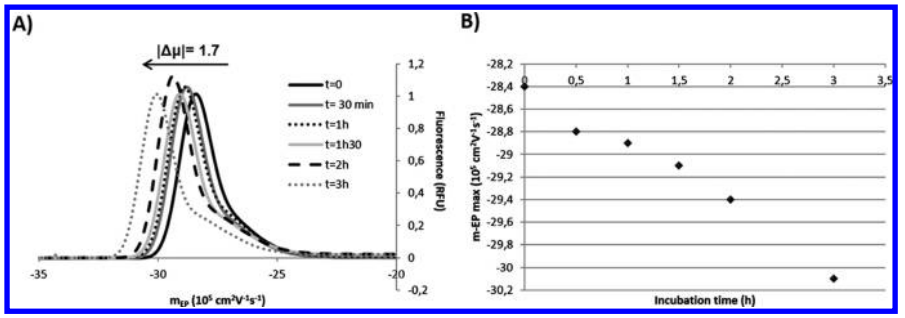

Figure 3. Study of nonspecific interactions between the nanoprobe and BSA by CZE. (A) Electropherograms obtained by the injection of mixtures QDs/BSA at different times of incubation (0−3 h), where a shift in QDs mobility is observed along the incubation time. (B) Plot showing the increase in the mobility of the nanoprobe after different times of exposition to BSA indicating a possible nonspecific interaction of the nanoprobe with BSA.

and nonspecific interactions with plasma proteins. In a first attempt, using the 10 mM carbonate buffer (Na_2CO_3/$NaHCO_3$) + 20 mM NaCl (pH 9.5) as the BGE, a colloidal stability study was done. Whereas the electrophoretic mobility of the P(SPP-4VIM)-QDs is $-15.7 \pm 0.1 \times 10^5$ cm^2 V^{-1} s^{-1}, the electrophoretic behavior of the different nano-objects shows that the addition of azide monomer or peptides to the polymer diminishes the global surface charge density, [-13.90 ± 0.06 and $-14.2 \pm 0.1 \times 10^5$ cm^2 V^{-1} s^{-1} for P(SPP-N_3-4VIM)-QD and RGD-QD, respectively]. No difference in mobility between RGD-QDs and RAD-QDs was observed, and the slight difference in m_{EP} observed between P(SPP-N_3-4VIM) and RGD/RAD-QDs could be explained by the inherent charges present on the peptide. The behavior of the different nano-objects was evaluated at different ionic strengths (30, 50, 70, and 120 mM). They present a classical electrophoretic behavior, with a decrease in the electrophoretic mobility while increasing the ionic strength, because of counter-ion electrostatic interactions (see Figure S7 in the Supporting Information). These results indicate that the zwitterionic polymers enable a good QD colloidal stability and size monodispersity at pH 9.5 in the 30−100 mM ionic strength range. Similar results were obtained in a 40 mM MOPS + 20 mM NaCl (pH 7.4) BGE, mimicking physiological conditions. These observations confirm the excellent colloidal stability of the QDs in different media (Figure S1).

Finally, to prove the antifouling properties of the designed polymer, nonspecific interactions of the nanoprobes with BSA protein molecules, a major constituent of blood serum, were evaluated by two different electrokinetic methods. ACE methodology is suitable to characterize fast interactions. It consists in the injection of the nanoprobe in a BGE containing the protein of study (BSA). Interactions were characterized at different BSA concentrations (0, 2, 10, and 20 μM), corresponding to similar studies carried out by other groups,[39,40] keeping constant the concentration of P(SPP-N_3-4VIM)-QDs at 6.5 μM. The BSA concentration is lower than the HSA concentration in blood (typically 500−750 μM), but this provides nonetheless useful information about QD−albumin interactions. In case of interactions, a shift in the electrophoretic mobility of QDs should be evidenced. Our results, however, do not show any change in the nanoprobe mobility, which remains similar to the mobility of the nanoprobes alone at $-29.1 \pm 0.3 \times 10^5$ cm^2 V^{-1} s^{-1}. No other peaks were observed, indicating that the QD population remained homogeneous. We can therefore conclude that there are no significant fast interactions between the QDs and BSA at the BSA concentration range evaluated.

We then tested slow adsorption of albumin onto the QDs. Here, the nanoprobes were incubated in a 50 μM BSA solution during different times (0, 0.5, 1, 1.5, 2, and 3 h), and the solutions were then analyzed by CZE using a BGE (40 mM MOPS + 20 mM NaCl pH 7.4) enriched with 10 μM BSA. Under all experienced conditions, the absorbance and fluorescence peaks corresponding to the QDs overlapped and provided similar mobilities (see Figure S8). The QDs showed a small shift toward more negative electrophoretic mobility with increasing incubation time, up to $|\Delta\mu| = 1.7 \times 10^5$ cm^2 V^{-1} s^{-1} after 3 h, corresponding to a ≈6% shift (Figure 3). The peak corresponding to free BSA remained unchanged ($m_{EP} = -14.3 \pm 0.3 \times 10^5$ cm^2 V^{-1} s^{-1}), and no new peak corresponding to QD/BSA aggregates appeared. This suggests that there should be a quite weak interaction between P(SPP-N_3-4VIM)-QDs and BSA under these experimental conditions. The very slight increase in the absolute mobility could indeed indicate a slight increase in the global surface charge density coming from the interaction with the BSA. This study highlights the remarkable antifouling properties of the zwitterionic polymers as was also observed for other similar polymers.[20,23] These results also demonstrate the great potential of CE as a reliable analytical tool to characterize protein−nanoparticle interactions as has been also demonstrated and revised in recent studies.[41,42] Thus, CE has an interesting place in this field because an increasing number of studies demonstrate that dynamic interactions of serum proteins with nanoprobes (so-called soft coronas) define their biological identity.

3.3. Probing Zwitterionic Polymer-Capped QDs as Optical Imaging Agents. *3.3.1. Cellular Viability Test: MTT.* Before envisioning a biological application, we performed an MTT metabolic assay on HeLa cells to evaluate the potential in vitro toxicity of both visible- and NIR-emitting QD nanoprobes. The metabolic activity of the cells was not significantly affected after 24 h of incubation even at high QD concentrations (Figure S9 in the Supporting Information, 5 μM: 119 ± 18% for vis-QDs and 100 ± 20% for NIR-QDs). This encouraging result enabled us to move to the in vitro and in vivo assays.

3.3.2. In Vitro Study of the Nanoprobe: Cellular Binding Test. Different parameters were evaluated to optimize the protocol for the specific targeting of cell membrane receptors ($\alpha_v\beta_3$ integrin), including (1) the concentration of the nanoprobe (50, 200, and 500 nM of QDs); (2) incubation time (30 min, 1 h, and 2 h) and temperature (37 and 4 °C);

DOI: 10.1021/acsami.8b04708
ACS Appl. Mater. Interfaces 2018, 10, 17107−17116

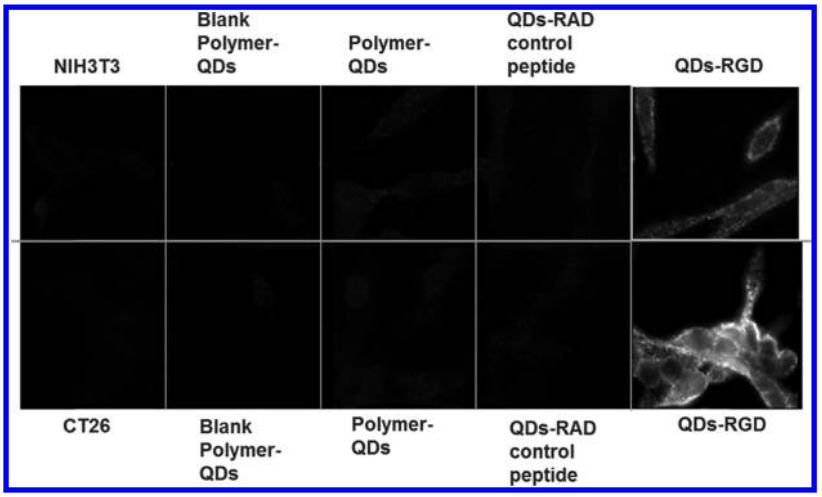

Figure 4. Specific targeting of integrins (membrane cell receptor of RGD) which are overexpressed in the case of carcinoma cells. Top line (control cell line series, NIH3T3) and bottom line (carcinoma cell line series, CT26). From left to right NIH3T3 or CT26 cells, respectively, P(SPP-4VIM)-QDs, P(SPP-N_3-4VIM)-QDs, RAD-QDs, and RGD-QDs.

and (3) modulation of the nanoprobe surface chemistry to avoid nonspecific interactions. Additionally, several controls of the nanoprobe (RGD-QDs) were tested: as surface chemistry controls, BP-QDs and polyN_3-QDs, and as peptide control, RAD-QDs, maintaining the same concentration in QDs for all of them.

The first attempt was focused on the selection of the concentration of QDs. As it is shown in Figure S10A of the Supporting Information, the fluorescence signal from QDs after 2 h of incubation at 37 °C is observed at the three tested concentrations. The selected concentration was 200 nM as it allowed us to visualize the fluorescent emission from the QDs, minimizing their internalization into the cells (phenomena which is clearly observed in the case of 500 nM). To figure out if it was possible to avoid the internalization of QDs, different incubation times and temperatures were explored. The optimal conditions were estimated for an incubation at 4 °C during 1 h (see Figure S10B), for the specific targeting of the $\alpha_v\beta_3$ integrin receptor, avoiding the internalization of the nanoprobe into the cells. However, nonspecific interactions of the nanoprobe surface chemistry with cells were observed. A possible hydrophobic interaction between the azido-bearing appendages and the cell membrane could be responsible of this fact. Thus, a blocking step of the azido function was incorporated into the preparation protocol of the nanoprobe. This blocking step consists in the saturation of the nanoprobe with the DBCO-NHS to finally obtain a carboxylic function at the surface of the nanoprobe. Once the azido function was blocked, the arms now incorporating a hydrophilic and negatively charged function, no non-specific interactions were observed anymore (see Figure S10C), highlighting the specific signal from the active nanoprobe RGD-QDs and allowing for improving the design of this nanoprobe.

Figure 4 shows the specific targeting of the $\alpha_v\beta_3$ integrins in both kinds of cellular lines (CT26 and NIH/3T3, carcinogenic and control cell lines, respectively) after 1 h of incubation with the nanoprobe at 4 °C, following the optimized protocol described in the Materials and Methods section. The $\alpha_v\beta_3$ integrin membrane receptor is overexpressed in the case of tumor cells, and consequently, a higher fluorescent emission signal is observed. As it is mentioned before, following this protocol, the nonspecific interactions from the polymer or the control peptide (RAD) with cell membrane are minimized. An active specific in vitro targeting is thus demonstrated, allowing us to pass to the in vivo study of the nanoprobe.

3.3.3. In Vivo Tumor Targeting. After the in vitro tests, we then tested the in vivo stealthiness of the nanoprobes which is an essential feature for potential tumor targeting. For such purpose, the tumor imaging capacity of QDs capped with the proposed surface chemistry was evaluated in a CT26 cancer mouse model. Three different NIR-emitting QD samples were prepared, namely nonfunctionalized P(SPP-N_3-4VIM)-, RGD-, and RAD-QDs. As mentioned before, based on our observations on cultured cells, residual N_3 functions were capped with DBCO−COOH linkers to reduce nonspecific interactions due to surface N_3 moieties. QDs were injected in the mouse tail vein. Fluorescence signals from normal tissue regions displayed exponential decays on the order of 120 ± 15 min (Figure S11), which we attribute to prolonged circulation of QDs in the blood stream. They finally accumulated in the liver because of normal capture by macrophages. The kinetics of liver uptake is recorded and is on the order of a few hours (Figure S12), which is consistent with the complementary observed circulation time in blood. This circulation time is considerably longer than for commercially available QDs, which are captured in a few minutes postinjection,[12−14] thanks to the very low nonspecific interactions of our QDs with proteins and cell membranes. This stealthiness feature of such nanoprobes is mandatory for further targeting studies and is therefore fulfilled by the developed QDs. We also note that the total whole-body fluorescence signal remained constant for a few days (Figure S13), which demonstrates the high chemical stability of these QDs in vivo. However, these results show a limited excretion of the nanoprobes that are preferentially accumulated in the liver, attributable to the capture by macrophages. This does not represent a strong limitation in the framework of applications in small animal models. Translating these probes to the clinical field would however require faster clearance of these nanoprobes.

Tumor uptake of RGD-functionalized QDs was visible initially, starting from 5 min postinjection and slowly decreased in the following hours and days (Figure 5). However, no significant differences in tumor uptake were observed between RGD-, RAD-, and nonfunctionalized-QDs. This suggests that,

DOI: 10.1021/acsami.8b04708
ACS Appl. Mater. Interfaces 2018, 10, 17107−17116

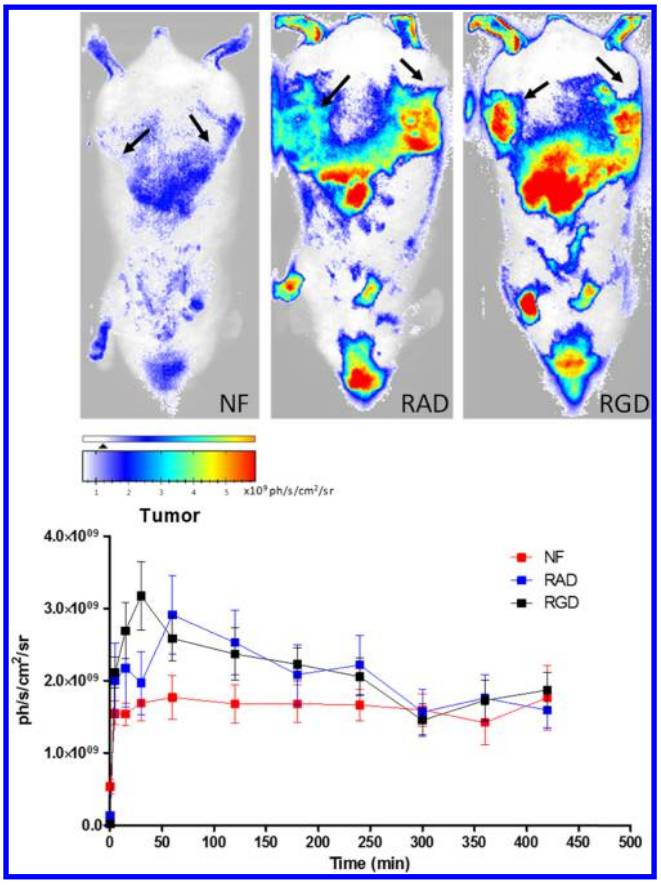

Figure 5. In vivo fluorescence imaging of mice bearing CT26 tumors (signaled with black arrows) after 3 h postintravenous injection of (from left to right): nonfunctionalized QD (NF), RAD-QD (control peptide), and RGD-QD (positive peptide); upper panel. Evolution of the tumor fluorescence signals as a function of time for RGD- (black), RAD- (blue), and nonfunctionalized-QDs (red); lower panel.

in this model, passive uptake is the main route by which QDs enter the tumor. This is also consistent with the observation that CT26 tumors grow fast and form leaky vessels prone to enhanced permeation and retention (EPR) effects.[32,43,44] This underscores the complexity of in vivo active tumor targeting: despite the demonstration of effective and specific in vitro recognition of the overexpressed $\alpha_v\beta_3$ integrin by RGD-QDs and the prolonged circulation of these QDs in the blood stream, active RGD/integrin recognition was overwhelmed by the strong passive tumor accumulation in vivo. This accumulation is attributable to a strong EPR effect in this highly vascularized tumor model, in agreement with other studies on CT26 tumors using different nanosystems.[45] Many physiological parameters may influence the active uptake of targeted nanoparticles into a solid tumor, including vascularization, blood vessel integrity, tumor microenvironment, etc. This stresses the importance of carefully designed control experiments to characterize active in vivo tumor targeting.

4. CONCLUSIONS

We have synthesized a novel clickable zwitterionic-imidazole block copolymer for the functionalization of visible and NIR-emitting QDs. We demonstrated the excellent stability and antifouling behavior of these probes, as well as easy bioorthogonal conjugation to small molecules or peptides. In addition, we have shown the potential of CE for the characterization of NP−biomolecule interactions, mimicking physiological conditions and allowing differentiation between weak and strong interactions. RGD-functionalized QDs can actively label tumor cells overexpressing $\alpha_v\beta_3$-integrin in vitro. For the first time, the in vivo blood circulation kinetics and tumor accumulation of sulfobetaine polymer-capped NIR-QDs were evaluated in mice. These QDs exhibit prolonged circulation in the blood stream and enable efficient fluorescence detection. Passive tumor labeling due to enhanced permeability and retention effect but no further specific RGD/integrin recognition was observed in vivo. These findings stress out the importance of taking into account angiogenesis and vascularization when designing actively targeted probes.

In a context where nanoparticle-based targeted drug delivery or theranostics into solid tumors is actively pursued, the optical properties of these QDs, their stability, and easy bioconjugation offer a novel tool to improve our understanding of in vivo active targeting. Furthermore, these clickable-zwitterionic copolymer capped-QDs can constitute a general platform for the design of original nanoprobes enlarging their applicability to the whole biomedical field thanks to their low toxicity, excellent antifouling properties, easy bioconjugation, and tunable fluorescent emission.

■ ASSOCIATED CONTENT

Supporting Information

The Supporting Information is available free of charge on the ACS Publications website at DOI: 10.1021/acsami.8b04708.

The protocols for the synthesis of both kind of QDs, the synthesis of azidomonomer, the ligand exchange process for the aqueous solubilization of QDs, optical properties of QDs (absorption and emission spectra, fluorescence lifetimes, and colloidal stability), FT-IR spectrum of the polymer, reagent chemical structures, ^{1}H NMR of the DBCO−peptide derivatization, capillary electrophoresis studies, MTT test, in vitro specific tumor targeting optimization, in vivo imaging, and calculation of the number of monomers per chain of polymer (PDF)

■ AUTHOR INFORMATION

Corresponding Author

*E-mail: anne.varenne@chimieparistech.psl.eu. Phone: (33) 1 44279007 (A.V.).

ORCID

Anne Varenne: 0000-0001-9711-1919

Present Addresses

#Soft Matter Laboratory, 1906 Soft Matter Laboratory, The Research Institute of Theoretical and Applied Physical Chemistry (INIFTA), CONICET-UNLP, 1906 La Plata, Argentina (M.T.).

¶Laboratoire Physico Chimie Curie, Laboratoire Physico Chimie Curie, Institut Curie, PSL Research University, CNRS UMR168, Sorbonne Universités, UPMC Univ Paris 06, Institut Pierre-Gilles de Gennes, 75005 Paris, France (L.T.-A.).

Author Contributions

The manuscript was written through contributions of all authors. All authors have given approval to the final version of the manuscript.

Funding

L.T.-A. acknowledges funding from PSL Research University through the project NanoBIM.

DOI: 10.1021/acsami.8b04708
ACS Appl. Mater. Interfaces 2018, 10, 17107−17116

Notes

The authors declare no competing financial interest.

■ ACKNOWLEDGMENTS

PSL Research University is kindly acknowledged for the financial support through the NanoBIM project. Mohamed Hanafi from the CNRS UMR 7615 at the ESPCI is kindly acknowledged by his assistance with the GPC analysis. In vivo imaging was performed at the Life Imaging Facility of Paris Descartes University [Plateforme Imageries du Vivant—PIV, partly supported by Région Ile-de-France (SESAM), CNRS, INSERM, and University Paris Descartes].

■ REFERENCES

(1) Mattoussi, H.; Palui, G.; Na, H. B. Luminescent quantum dots as platforms for probing in vitro and in vivo biological processes. *Adv. Drug Deliv. Rev.* **2012**, *64*, 138−166.
(2) Dahan, M.; Lévi, S.; Luccardini, C.; Rostaing, P.; Riveau, B.; Triller, A. Diffusion dynamics of glycine receptors revealed by single-quantum dot tracking. *Science* **2003**, *302*, 442−445.
(3) Michalet, X.; Pinaud, F. F.; Bentolila, L. A.; Tsay, J. M.; Doose, S.; Li, J. J.; Sundaresan, G.; Wu, A. M.; Gambhir, S. S.; Weiss, S. Quantum Dots for Live Cells, in Vivo Imaging, and Diagnostics. *Science* **2005**, *307*, 538−544.
(4) Chan, W. C. W.; Maxwell, D. J.; Gao, X.; Bailey, R. E.; Han, M.; Nie, S. Luminescent quantum dots for multiplexed biological detection and imaging. *Curr. Opin. Biotechnol.* **2002**, *13*, 40−46.
(5) Kim, S.; Lim, Y. T.; Soltesz, E. G.; De Grand, A. M.; Lee, J.; Nakayama, A.; Parker, J. A.; Mihaljevic, T.; Laurence, R. G.; Dor, D. M.; Cohn, L. H.; Bawendi, M. G.; Frangioni, J. V. Near-infrared fluorescent type II quantum dots for sentinel lymph node mapping. *Nat. Biotechnol.* **2004**, *22*, 93−97.
(6) Cassette, E.; Helle, M.; Bezdetnaya, L.; Marchal, F.; Dubertret, B.; Pons, T. Design of new quantum dot materials for deep tissue infrared imaging. *Adv. Drug Deliv. Rev.* **2013**, *65*, 719−731.
(7) Li, L.; Daou, T. J.; Texier, I.; Chi, T. T. K.; Liem, N. Q.; Reiss, P. Highly Luminescent CuInS2/ZnS Core/Shell Nanocrystals: Cadmium-Free Quantum Dots for In Vivo Imaging. *Chem. Mater.* **2009**, *21*, 2422−2429.
(8) Pons, T.; Pic, E.; Lequeux, N.; Cassette, E.; Bezdetnaya, L.; Guillemin, F.; Marchal, F.; Dubertre, B. Cadmium-Free CuInS2/ZnS Quantum Dots for Sentinel Lymph Node Imaging with Reduced Toxicity. *ACS Nano* **2010**, *4*, 2531−2538.
(9) Helle, M.; Cassette, E.; Bezdetnaya, L.; Pons, T.; Leroux, A.; Plénat, F.; Guillemin, F.; Dubertret, B.; Marchal, F. Visualisation of Sentinel Lymph Node with Indium-Based near Infrared Emitting Quantum Dots in a Murine Metastatic Breast Cancer Model. *PLoS ONE* **2012**, *7*, No. e44433.
(10) Bouccara, S.; Fragola, A.; Giovanelli, E.; Sitbon, G.; Lequeux, N.; Pons, T.; Loriette, V. Time-gated cell imaging using long lifetime near-infrared-emitting quantum dots for autofluorescence rejection. *J. Biomed. Opt.* **2014**, *19*, 051208.
(11) Wu, X.; Liu, H.; Liu, J.; Haley, K. N.; Treadway, J. A.; Larson, J. P.; Ge, N.; Peale, F.; Bruchez, M. P. Immunofluorescent labeling of cancer marker Her2 and other cellular targets with semiconductor quantum dots. *Nat. Biotechnol.* **2003**, *21*, 41−46.
(12) Schipper, M. L.; Cheng, Z.; Lee, S.-W.; Bentolila, L. A.; Iyer, G.; Rao, J.; Chen, X.; Wu, A. M.; Weiss, S.; Gambhir, S. S. MicroPET-based biodistribution of quantum dots in living mice. *J Nucl. Med.* **2007**, *48*, 1511−1518.
(13) Ballou, B.; Lagerholm, B. C.; Ernst, L. A.; Bruchez, M. P.; Waggoner, A. S. Noninvasive imaging of quantum dots in mice. *Bioconjugate Chem.* **2004**, *15*, 79−86.
(14) Morgan, N. Y.; English, S.; Chen, W.; Chernomordik, V.; Russo, A.; Smith, P. D.; Gandjbakhche, A. Real time in vivo non-invasive optical imaging using near-infrared fluorescent quantum dots. *Acad. Radiol.* **2005**, *12*, 313−323.
(15) Yildiz, I.; Deniz, E.; McCaughan, B.; Cruickshank, S. F.; Callan, J. F.; Raymo, F. M. Hydrophilic CdSe−ZnS Core−Shell Quantum Dots with Reactive Functional Groups on Their Surface. *Langmuir* **2010**, *26*, 11503−11511.
(16) Stewart, M. H.; Susumu, K.; Mei, B. C.; Medintz, I. L.; Delehanty, J. B.; Blanco-Canosa, J. B.; Dawson, P. E.; Mattoussi, H. Multidentate Poly(ethylene glycol) Ligands Provide Colloidal Stability to Semiconductor and Metallic Nanocrystals in Extreme Conditions. *J. Am. Chem. Soc.* **2010**, *132*, 9804−9813.
(17) Liu, W.; Greytak, A. B.; Lee, J.; Wong, C. R.; Park, J.; Marshall, L. F.; Jiang, W.; Curtin, P. N.; Ting, A. Y.; Nocera, D. G.; Fukumura, D.; Jain, R. K.; Bawendi, M. G. Compact Biocompatible Quantum Dots via RAFT-Mediated Synthesis of Imidazole-Based Random Copolymer Ligand. *J. Am. Chem. Soc.* **2010**, *132*, 472−483.
(18) Susumu, K.; Oh, E.; Delehanty, J. B.; Pinaud, F.; Gemmill, K. B.; Walper, S.; Breger, J.; Schroeder, M. J.; Stewart, M. H.; Jain, V.; Whitaker, C. M.; Huston, A. L.; Medintz, I. L. A New Family of Pyridine-Appended Multidentate Polymers As Hydrophilic Surface Ligands for Preparing Stable Biocompatible Quantum Dots. *Chem. Mater.* **2014**, *26*, 5327−5344.
(19) García, K. P.; Zarschler, K.; Barbaro, L.; Barreto, J. A.; O'Malley, W.; Spiccia, L.; Stephan, H.; Graham, B. Zwitterionic-coated "stealth" nanoparticles for biomedical applications: recent advances in countering biomolecular corona formation and uptake by the mononuclear phagocyte system. *Small* **2014**, *10*, 2516−2529.
(20) Giovanelli, E.; Muro, E.; Sitbon, G.; Hanafi, M.; Pons, T.; Dubertret, B.; Lequeux, N. Highly Enhanced Affinity of Multidentate versus Bidentate Zwitterionic Ligands for Long-Term Quantum Dot Bioimaging. *Langmuir* **2012**, *28*, 15177−15184.
(21) Zhan, N.; Palui, G.; Safi, M.; Ji, X.; Mattoussi, H. Multidentate zwitterionic ligands provide compact and highly biocompatible quantum dots. *J. Am. Chem. Soc.* **2013**, *135*, 13786−13795.
(22) Van Andel, E.; de Bus, I.; Tijhaar, E. J.; Smulders, M. M. J.; Savelkoul, H. F. J.; Zuilhof, H. Highly specific binding on antifouling zwitterionic polymer-coated microbeads as measured by flow cytometry. *ACS Appl. Mater. Interfaces* **2017**, *9*, 38211−38221.
(23) Dembele, F.; Tasso, M.; Trapiella-Alfonso, L.; Xu, X.; Hanafi, M.; Lequeux, N.; Pons, T. Zwitterionic-silane copolymer for ultra stable and bright biomolecular probes based on fluorescent quantum dot nanoclusters. *ACS Appl. Mater. Interfaces* **2017**, *9*, 18161−18169.
(24) Susumu, K.; Oh, E.; Delehanty, J. B.; Blanco-Canosa, J. B.; Johnson, B. J.; Jain, V.; Hervey, W. J.; Algar, W. R.; Boeneman, K.; Dawson, P. E.; Medintz, I. L. Multifunctional compact zwitterionic ligands for preparing robust biocompatible semiconductor quantum dots and gold nanoparticles. *J. Am. Chem. Soc.* **2011**, *133*, 9480−9496.
(25) Tasso, M.; Giovanelli, E.; Zala, D.; Bouccara, S.; Fragola, A.; Hanafi, M.; Lenkei, Z.; Pons, T.; Lequeux, N. Sulfobetaine-Vinylimidazole Block Copolymers: A Robust Quantum Dot Surface Chemistry Expanding Bioimaging's Horizons. *ACS Nano* **2015**, *9*, 11479−11489.
(26) Schipper, M. L.; Iyer, G.; Koh, A. L.; Cheng, Z.; Ebenstein, Y.; Aharoni, A.; Keren, S.; Bentolila, L. A.; Li, J.; Rao, J.; et al. Particle size, surface coating, and PEGylation influence the biodistribution of quantum dots in living mice. *Small* **2009**, *5*, 126−134.
(27) Yong, K.-T.; Hu, R.; Roy, I.; Ding, H.; Vathy, L. A.; Bergey, E. J.; Mizuma, M.; Maitra, A.; Prasad, P. N. Tumor targeting and imaging in live animals with functionalized semiconductor quantum dots. *ACS Appl. Mater. Interfaces* **2009**, *1*, 710−719.
(28) Moses, J. E.; Moorhouse, A. D. The growing applications of click chemistry. *Chem. Soc. Rev.* **2007**, *36*, 1249−1262.
(29) Li, J. J.; Wang, Y. A.; Guo, W. Z.; Keay, J. C.; Mishima, T. D.; Johnson, M. B.; Peng, X. G. Large-scale synthesis of nearly monodisperse CdSe/CdS core/shell nanocrystals using air-stable reagents via successive ion layer adsorption and reaction. *J. Am. Chem. Soc.* **2003**, *125*, 12567−12575.
(30) Yang, Y. A.; Wu, H.; Williams, K. R.; Cao, Y. C. Synthesis of CdSe and CdTe Nanocrystals without Precursor Injection. *Angew. Chem., Int. Ed.* **2005**, *44*, 6712−6715.

DOI: 10.1021/acsami.8b04708
ACS Appl. Mater. Interfaces 2018, 10, 17107−17116

(31) Monteiro-Riviere, N. A.; Inman, A. O.; Zhang, L. W. Limitations and relative utility of screening assays to assess engineered nanoparticle toxicity in a human cell line. *Toxicol. Appl. Pharmacol.* **2009**, *234*, 222−235.
(32) Seguin, J.; Doan, B.-T.; Ossa, H. L.; Jugé, L.; Gennisson, J.-L.; Tanter, M.; Mignet, N. Evaluation of Non radiative Clinical Imaging Techniques for the Longitudinal Assessment of Tumour Growth in Murine CT26 Colon Carcinoma. *Int. J. Mol. Imaging* **2013**, *2013*, 983534.
(33) Frangioni, J. V. In vivo near-infrared fluorescence imaging. *Curr. Opin. Chem. Biol.* **2003**, *7*, 626−634.
(34) Bolley, J.; Guenin, E.; Lievre, N.; Lecouvey, M.; Soussan, M.; Lalatonne, Y.; Motte, L. Carbodiimide versus Click Chemistry for Nanoparticle Surface Functionalization: A Comparative Study for the Elaboration of Multimodal Superparamagnetic Nanoparticles Targeting $\alpha v\beta 3$ Integrins. *Langmuir* **2013**, *29*, 14639−14647.
(35) Chen, Y.; Xianyu, Y.; Wu, J.; Yin, B.; Jiang, X. Click Chemistry-Mediated Nanosensors for Biochemical Assays. *Theranostics* **2016**, *6*, 969−985.
(36) Bernardin, A.; Cazet, A.; Guyon, L.; Delannoy, P.; Vinet, F.; Bonnaffé, D.; Texier, I. Copper-Free Click Chemistry for Highly Luminescent Quantum Dot Conjugates: Application to in vivo Metabolic Imaging. *Bioconjugate Chem.* **2010**, *21*, 583−588.
(37) Schieber, C.; Bestetti, A.; Lim, J. P.; Ryan, A. D.; Nguyen, T.-L.; Eldridge, R.; White, A. R.; Gleeson, P. A.; Donnelly, P. S.; Williams, S. J.; Mulvaney, P. Conjugation of Transferrin to Azide-Modified CdSe/ZnS Core−Shell Quantum Dots using Cyclooctyne Click Chemistry. *Angew. Chem., Int. Ed.* **2012**, *51*, 10523−10527.
(38) Wang, W.; Kapur, A.; Ji, X.; Zeng, B.; Mishra, D.; Mattoussi, H. Multifunctional and High Affinity Polymer Ligand that Provides Bio-Orthogonal Coating of Quantum Dots. *Bioconjugate Chem.* **2016**, *27*, 2024−2036.
(39) Wang, J.; Li, J.; Teng, Y.; Hu, W.; Chai, H.; Li, J.; Wang, C.; Qiu, L.; Jiang, P. Studies on multivalent interactions of quantum dots − protein self-assemble using fluorescence coupled capillary electrophoresis. *J. Nano Res.* **2014**, *16*, 2487.
(40) Boulos, S. P.; Davis, T. A.; Yang, J. A.; Lohse, S. E.; Alkilany, A. M.; Holland, L. A.; Murphy, C. J. Nanoparticle−Protein Interactions: A Thermodynamic and Kinetic Study of the Adsorption of Bovine Serum Albumin to Gold Nanoparticle Surfaces. *Langmuir* **2013**, *29*, 14984.
(41) Ramírez-García, G.; d'Orlyé, F.; Gutiérrez-Granados, S.; Martínez-Alfaro, M.; Mignet, N.; Richard, C.; Varenne, A. Electrokinetic Hummel-Dreyer characterization of nanoparticle-plasma protein corona: the non-specific interactions between PEG-modified persistent luminescent nanoparticles and albumin. *Colloids Surf., B* **2017**, *159*, 437−444.
(42) Trapiella-Alfonso, L.; Ramírez-García, G.; d'Orlyé, F.; Varenne, A. Electromigration separation methodologies for the characterization of nanoparticles and the evaluation of their behaviour in biological systems. *Trac. Trends Anal. Chem.* **2016**, *84*, 121−130.
(43) Mei, K.-C.; Bai, J.; Lorrio, S.; Wang, J. T.-W.; Al-Jamal, K. T. Investigating the effect of tumor vascularization on magnetic targeting in vivo using retrospective design of experiment. *Biomaterials* **2016**, *106*, 276−285.
(44) Schleich, N.; Sibret, P.; Danhier, P.; Ucakar, B.; Laurent, S.; Muller, R. N.; Jérôme, C.; Gallez, B.; Préat, V.; Danhier, F. Dual anticancer drug/superparamagnetic iron oxide-loaded PLGA-based nanoparticles for cancer therapy and magnetic resonance imaging. *Int. J. Pharm.* **2013**, *447*, 94−101.
(45) Kunjachan, S.; Pola, R.; Gremse, F.; Theek, B.; Ehling, J.; Moeckel, D.; Hermanns-Sachweh, B.; Pechar, M.; et al. Passive versus Active tumor targeting using RGD- and NGR-modified polymeric nanomedicines. *Nano Lett.* **2014**, *14*, 972−981.

DOI: 10.1021/acsami.8b04708
ACS Appl. Mater. Interfaces 2018, 10, 17107−17116